

Supporting Information for

Observation of topological flat bands in the kagome

semiconductor Nb₃Cl₈

Zhenyu Sun,^{1,4} Hui Zhou,^{1,4} Cuixiang Wang,^{1,4} Shiv Kumar,^{1,4} Daiyu Geng,^{1,4} Shaosheng Yue,^{1,4} Xin Han,^{1,4} Yuya Haraguchi,³ Kenya Shimada,² Peng Cheng,^{1,4} Lan Chen,^{1,4,5} Youguo Shi,^{1,4,5,6} Kehui Wu,^{1,4,5} Sheng Meng,^{1,4} and Baojie Feng^{1,4}

¹Institute of Physics, Chinese Academy of Sciences, Beijing 100190, China

²Hiroshima Synchrotron Radiation Center, Hiroshima University, 2-313 Kagamiyama, Higashi-Hiroshima 739-0046, Japan

³Department of Applied Physics and Chemical Engineering, Tokyo University of Agriculture and Technology, Koganei, Tokyo 184-8588, Japan

⁴School of Physical Sciences, University of Chinese Academy of Sciences, Beijing 100049, China

⁵Songshan Lake Materials Laboratory, Dongguan, Guangdong 523808, China

⁶Center of Materials Science and Optoelectronics Engineering, University of Chinese Academy of Sciences, Beijing 100049, China

1. Generalizing the destructive phase interference to a breathing kagome lattice

To confirm our analysis, we performed TB calculations. The real-space wavefunctions in breathing kagome lattice take the form:

$$\psi = \frac{1}{\sqrt{6}} \sum_{j=1}^6 (-1)^j \phi_j.$$

where ϕ_j is the s -orbital wavefunction at the j^{th} corner of the hexagon and j is sorted in the clockwise or anticlockwise direction. By transforming the real-space wavefunctions to the momentum space, we obtained the Bloch states:

$$\psi_{\mathbf{k}} = C \begin{pmatrix} e^{ik\frac{1}{6}(\delta a_1 - \delta a_3)} \sin \frac{ka_2}{2} \\ e^{ik\frac{1}{6}(\delta a_2 - \delta a_1)} \sin \frac{ka_3}{2} \\ e^{ik\frac{1}{6}(\delta a_3 - \delta a_2)} \sin \frac{ka_1}{2} \end{pmatrix}$$

where C is the normalization factor, a_i is the lattice vector, and δa_i is an a_i - directional vector with the length being the difference of two kinds of bonds. The Hamiltonian of the breathing Kagome lattice takes the form:

$$H = - \begin{pmatrix} 0 & t_1 e^{-ika_{1l}} + t_2 e^{ika_{1s}} & t_1 e^{ika_{3l}} + t_2 e^{-ika_{3s}} \\ t_1 e^{ika_{1l}} + t_2 e^{-ika_{1s}} & 0 & t_1 e^{-ika_{2l}} + t_2 e^{ika_{2s}} \\ t_1 e^{-ika_{3l}} + t_2 e^{ika_{3s}} & t_1 e^{ika_{2l}} + t_2 e^{-ika_{2s}} & 0 \end{pmatrix}$$

where t_1 and t_2 are the nearest neighbor hopping in the big and small triangles, respectively, a_{il} and a_{is} are the a_i -directional vector with the length being the long and short bonds, respectively. We find that ψ_k is the eigenfunction of the flat band by solving the eigenfunction of the Hamiltonian H . Therefore, the breathing kagome lattice also hosts topological flat bands that arise from the destructive phase interference in real space.

2. Inversion symmetry breaking induced gap opening in the kagome lattice

Here, we demonstrate that the band gap opening at the K point of the breathing kagome lattice ($P\bar{6}m2$) with respect to the kagome lattice ($P\frac{6}{m}mm$) is driven by the inversion symmetry breaking. For the kagome lattice, the little group at the K point is D_{3h} and the doubly degenerate bands at the K point, *i.e.*, the Dirac point, are ensured by the 2D irreducible representation of D_{3h} . For the breathing kagome lattice, due to the inversion symmetry breaking, the little group at the K point decreases to C_{3h} , whose irreducible representations are all 1D. Therefore, the doubly degenerate bands at the K point are gapped out.

Monolayer Nb_3Cl_8 has a space group of $P3m1$ without inversion symmetry. This is the reason for the gap opening at the K point. It should be noted that z -directed mirror symmetry is also broken in monolayer Nb_3Cl_8 , which is not necessary for the gap opening at the K point.

3. Determining the magnetic ground state of monolayer Nb_3Cl_8

To determine the magnetic ground state of monolayer Nb_3Cl_8 , we calculated the free energy of five types of magnetic orderings: the paramagnetic (PARA) ordering, antiferromagnetic (AFM) ordering, x -, y -, and z -directed FM orderings, as shown in Table S1. The primitive cell was used in the calculations. For the AFM ordering, the magnetic moments of two Nb atoms in the primitive cell are along the z direction, while that of the third one is along the negative z direction. We find that the free energies of PARA and AFM orderings are higher than those of the FM orderings, indicating that monolayer Nb_3Cl_8 has a FM ground state. Among the three FM orderings, the free energy of x -directed FM ordering is the lowest, indicating an easy magnetization axis along the x direction.

The band structure of Nb_3Cl_8 in the ferromagnetic state is shown in Fig. S1. Because of the magnetic exchange interaction, all the bands in the proximity of the

Fermi level are spin split, including the topological flat bands.

Table S1: Calculated free energies of four magnetic states of Nb_3Cl_8 . The x direction corresponds to the a axis in Fig. 1f of the main text.

	PARA	AFM	x -FM	y -FM	z -FM
Energy (eV)	-58.961276	-58.999540	-58.999607	-58.999600	-58.999600

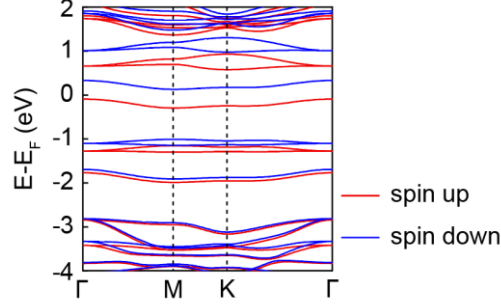


Fig. S1: The calculated band structures of monolayer Nb_3Cl_8 in the ferromagnetic states without SOC. The magnetization direction is along x .

4. Topological properties of the flat bands in Nb_3Cl_8 .

To confirm the topology of the flat band in Nb_3Cl_8 , we first calculate the band structures of Nb_3Cl_8 in the paramagnetic state including spin-orbit coupling (SOC), as shown in Fig. S2(a). The quadratic touching point at Γ between the flat band γ and the dispersive band β is gapped out after inclusion of SOC. We further calculated the edge spectrum of Nb_3Cl_8 with a semi-infinite geometry, as shown in Fig. S2(b). Helical edge states emerge in the bulk gap, indicating a Z_2 topological invariant of the SOC-induced gap. We also calculated the Z_2 topological invariant by the Wilson loop method, as shown in Fig. S2(c). These results confirm the topological nature of the flat band.

We then discuss the topological properties of Nb_3Cl_8 in the ferromagnetic state. When SOC is included, the touching points at Γ between the flat band γ and the dispersive band β are gapped out for both spin-up and spin-down channels, as shown in Fig. S3(a). We further calculated the edge spectrum of Nb_3Cl_8 with a semi-infinite geometry. As shown in Fig. S3(b) and S3(c), chiral edge states emerge in both gaps, indicating a Chern topological invariant of each SOC-induced gap. The total Chern numbers for the lower and upper gaps are -1 and 1, respectively. The opposite Chern numbers indicate that the spin and transport directions of the edge states are opposite in the two gaps.

In conclusion, the topological flat band supports a nontrivial Z_2 topological invariant in the paramagnetic state and will split into two topological flat bands with opposite Chern numbers in the ferromagnetic state.

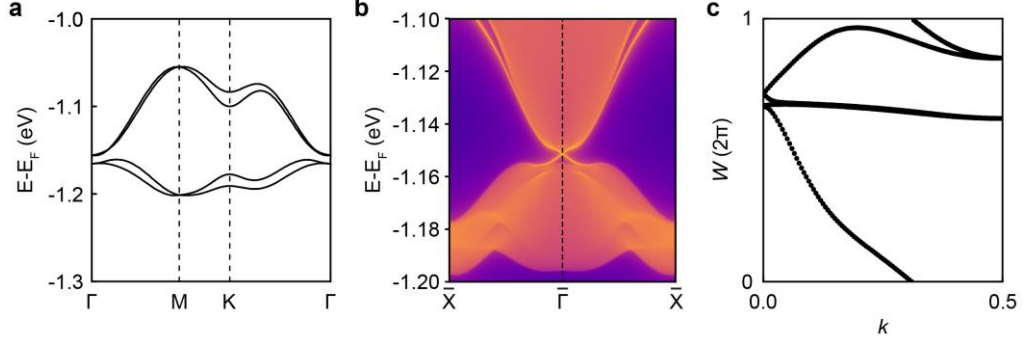


Fig. S2: Topological properties of monolayer Nb_3Cl_8 in the paramagnetic state. (a) Calculated band structures of monolayer Nb_3Cl_8 including SOC. (b) Calculated edge spectrum of Nb_3Cl_8 based on a semi-infinite geometry. (c) Calculated Z_2 topological invariants using the Wilson loop method.

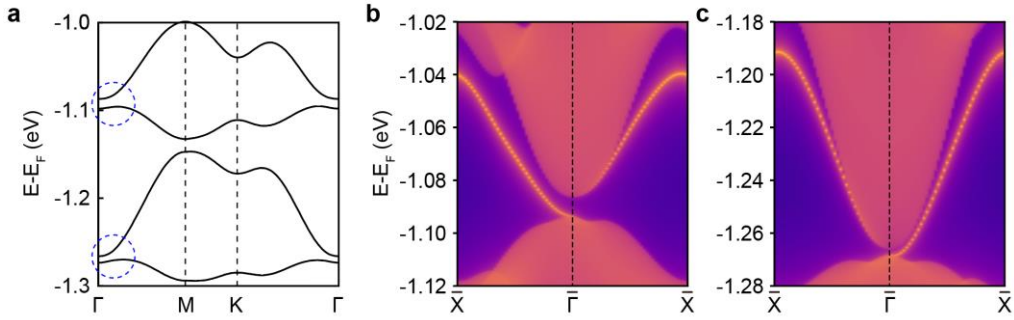


Fig. S3: Topological properties of monolayer Nb_3Cl_8 in the ferromagnetic state. (a) Calculated band structures of monolayer Nb_3Cl_8 considering SOC. Blue dashed circles indicate SOC-induced gaps. (b,c) Calculated edge spectrum of Nb_3Cl_8 based on a semi-infinite geometry for the upper and lower gaps, respectively.

5. Orbital and symmetry analysis of the flat band

To understand the topological nature of the flat band, we projected the band structures of monolayer Nb_3Cl_8 to the dz^2 , dx^2y^2/dxy , and dxz/dyz orbitals, respectively, as shown in Fig. S4. The α and δ bands are mainly contributed by the dz^2 orbital. Since these two bands have even parity, we can exclude these two bands from kagome flat bands. The β and γ bands are contributed by multiple d orbitals. Since the β band have even symmetry and have dz^2 orbital components, we can also exclude it from the kagome flat band. Therefore, the only possible one is the γ band that has odd parity. After comparing with Ref. [1], we find that dx^2y^2/dxy orbital of the γ band corresponds to ψ_3 in Fig. 2(b) of that paper which is phase destructive interfering. It should be noted that the dz^2 orbital components in the γ band is also phase destructive interfering.

Therefore, we can unambiguously prove that the γ band is the kagome-derived flat band.

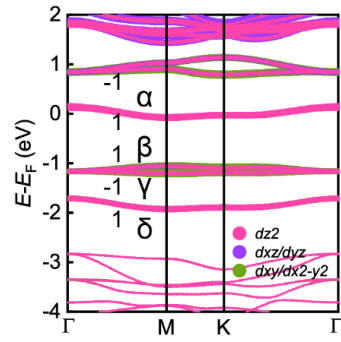


Fig. S4: Calculated partial density of states of monolayer Nb₃Cl₈. The parity of the mirror operator along Γ -M is labelled by “+” and “-” near each band.

References

- [1] Ge, H.; Xie, Y.; Chen, Y. d-orbital-frustration-induced ferromagnetic monolayer Cu₃O₂. *Phys. B: Condens. Matter.* 2020, 577, 411526.